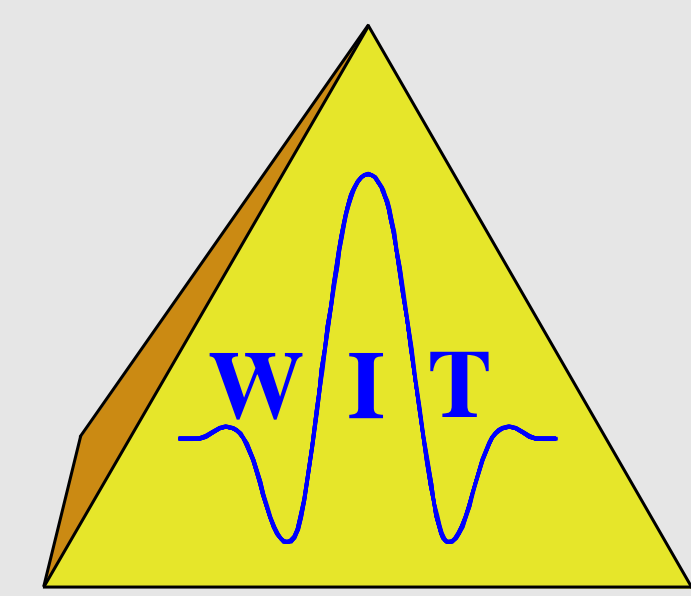


Common-Reflection-Surface Stack: an Attribute Analysis

Jürgen Mann, German Höcht, Rainer Jäger, and Peter Hubral
Geophysical Institute, University of Karlsruhe



Summary

The common reflection surface (CRS) stack is a macro velocity model independent method to simulate zero-offset (ZO) sections from multi-coverage seismic reflection data for 2-D media.

The CRS stacking operator depends on attributes of hypothetical wavefronts observed at the surface that allow to perform a subsequent inversion.

The CRS stacking operators fitting best to actual reflection events in the data set have to be determined by coherency analysis. The main task is the determination of these operators by variation of the attributes in a reasonable computation time preserving a sufficient accuracy.

Wavefront attributes

The CRS stacking operator is based on wavefront attributes of two so-called *eigenwaves*. These eigenwaves are provided by the hypothetical experiments illustrated in Figure 1 for a model with three homogeneous layers.

A point source at R provides the so-called *normal incidence point (NIP)* wave (Figure 1a), whereas an exploding reflector experiment yields the so-called *normal wave* (Figure 1b).

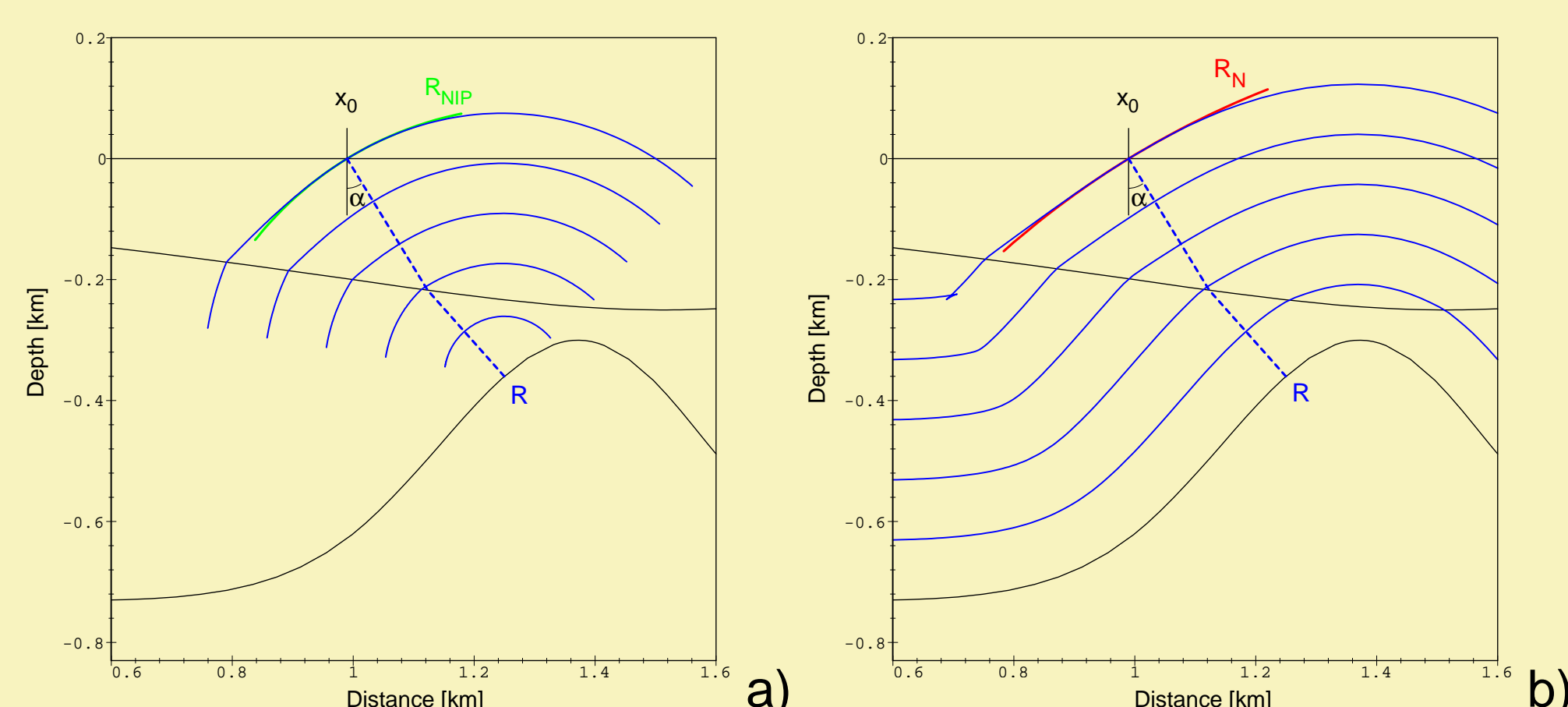


Figure 1: Two hypothetical experiments: a) *NIP* wave for a point source at R, b) *normal* wave for an exploding reflector. The central ray is depicted in blue dashes.

A circular approximation of these wavefronts in a vicinity of x_0 at the surface can be represented by the following set of parameters:

- α , the angle of emergence of the central ray
- R_{NIP} , the radius of curvature of the *NIP* wave
- R_N , the radius of curvature of the *normal* wave

CRS stacking operator

The CRS stacking operator is given in a parametric form depending on the three wavefront attributes α , R_{NIP} , and R_N . Its more convenient hyperbolic Taylor expansion for a point (t_0, x_0) reads

$$t^2(\Delta x, h) = \left(t_0 + \frac{2 \sin \alpha \Delta x}{v_0} \right)^2 + \frac{2 t_0 \cos^2 \alpha}{v_0} \left(\frac{\Delta x^2}{R_N} + \frac{h^2}{R_{NIP}} \right),$$

where h denotes the half offset and Δx the distance between x_0 and the respective common midpoint (CMP).

In the CMP gather (i. e. $\Delta x = 0$), the operator reduces to

$$t^2(h) = t_0^2 + \frac{4 h^2}{v_{NMO}^2} \quad \text{with} \quad v_{NMO}^2 = 2 v_0 R_{NIP} / (t_0 \cos^2 \alpha).$$

Please note that the squared stacking velocity v_{NMO}^2 may also be negative.

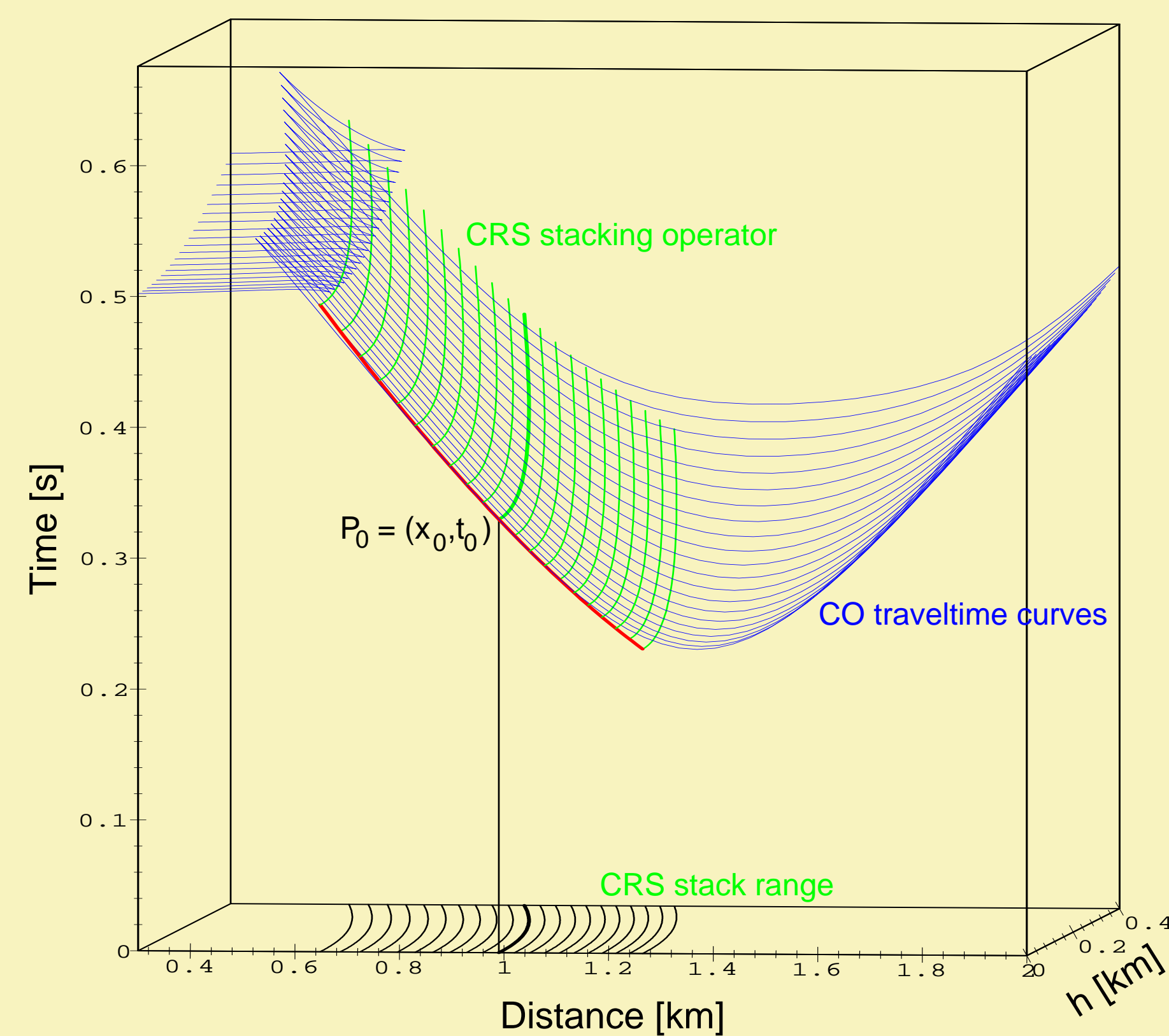


Figure 2: Forward calculated traveltimes surface (blue) compared to the CRS stacking operator (green) according to the true (model derived) attributes. In the zero-offset plane the operator is depicted in red. The CRS stack range corresponds to a paraxial vicinity of the central ray.

Model

We simulated a multi-coverage data set containing all primary events for the model shown in Figure 3. It consists of six homogeneous layers separated by five dome-like interfaces. The wavelet is a Ricker wavelet with a peak frequency of 30 Hz.

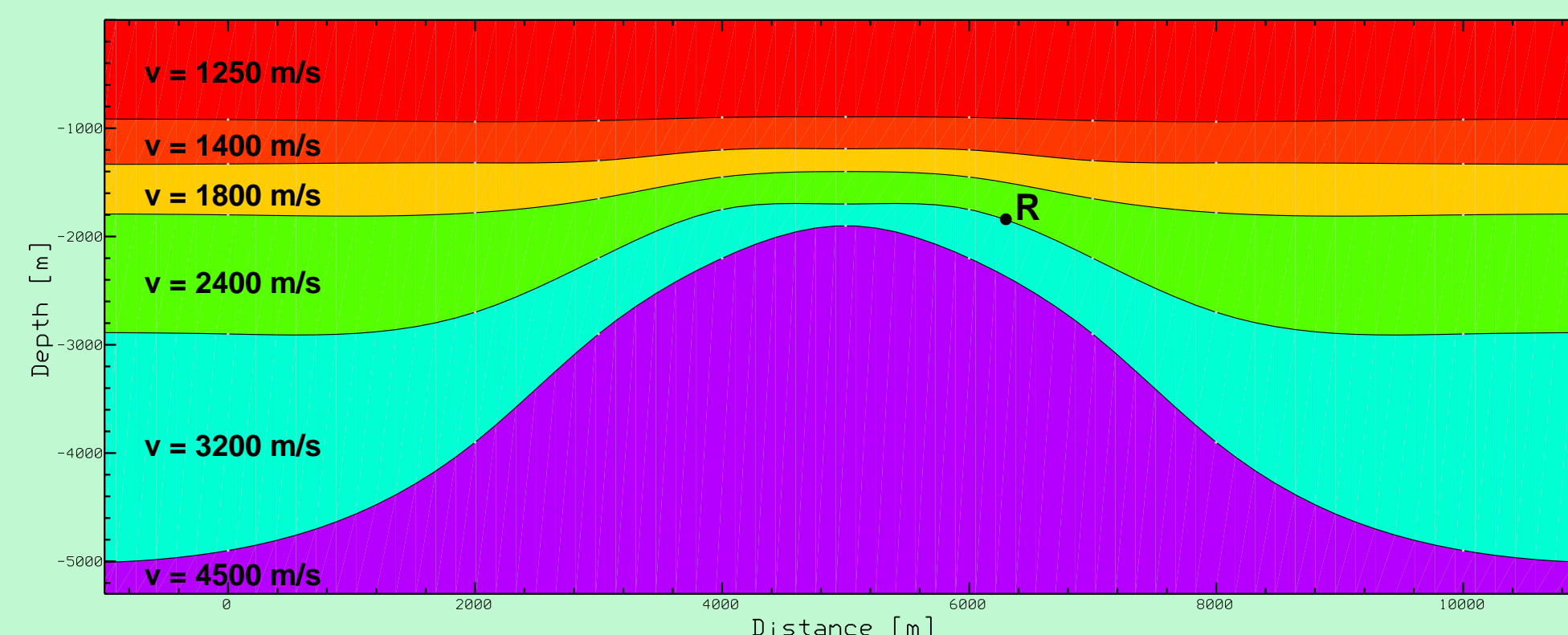


Figure 3: Model with homogeneous layers and dome-like interfaces.

For the further processing we added noise with a S/N ratio of 4. The zero-offset section of this data set is depicted in Figure 4.

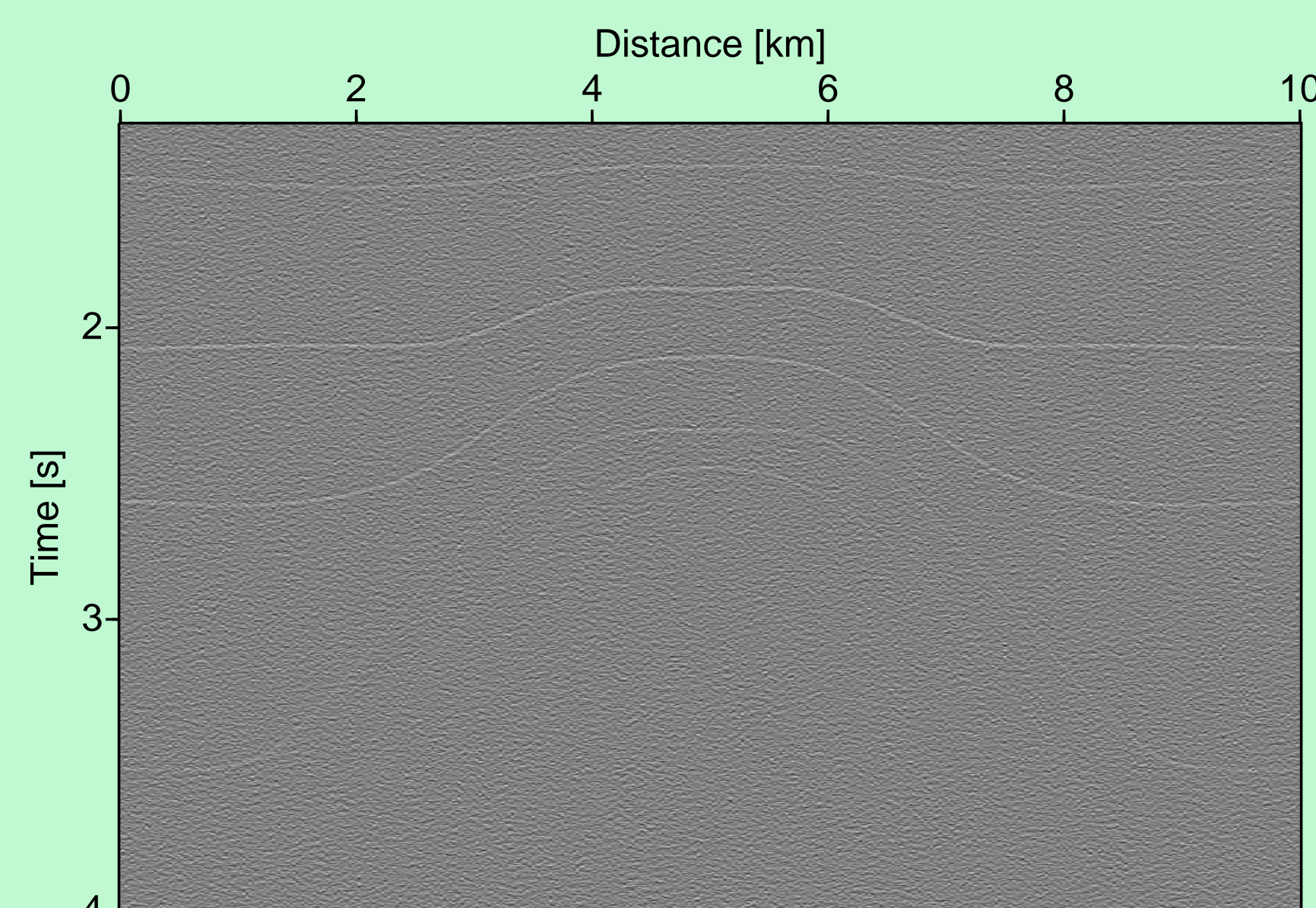


Figure 4: Zero-offset section of the simulated multi-coverage data set.

Determination of the attributes

To determine the optimum stacking operator we look for the wavefield attributes yielding the highest coherency value along the respective operator. Figure 5 illustrates the coherency in the three-parametric attribute domain for one selected point situated on an interface.

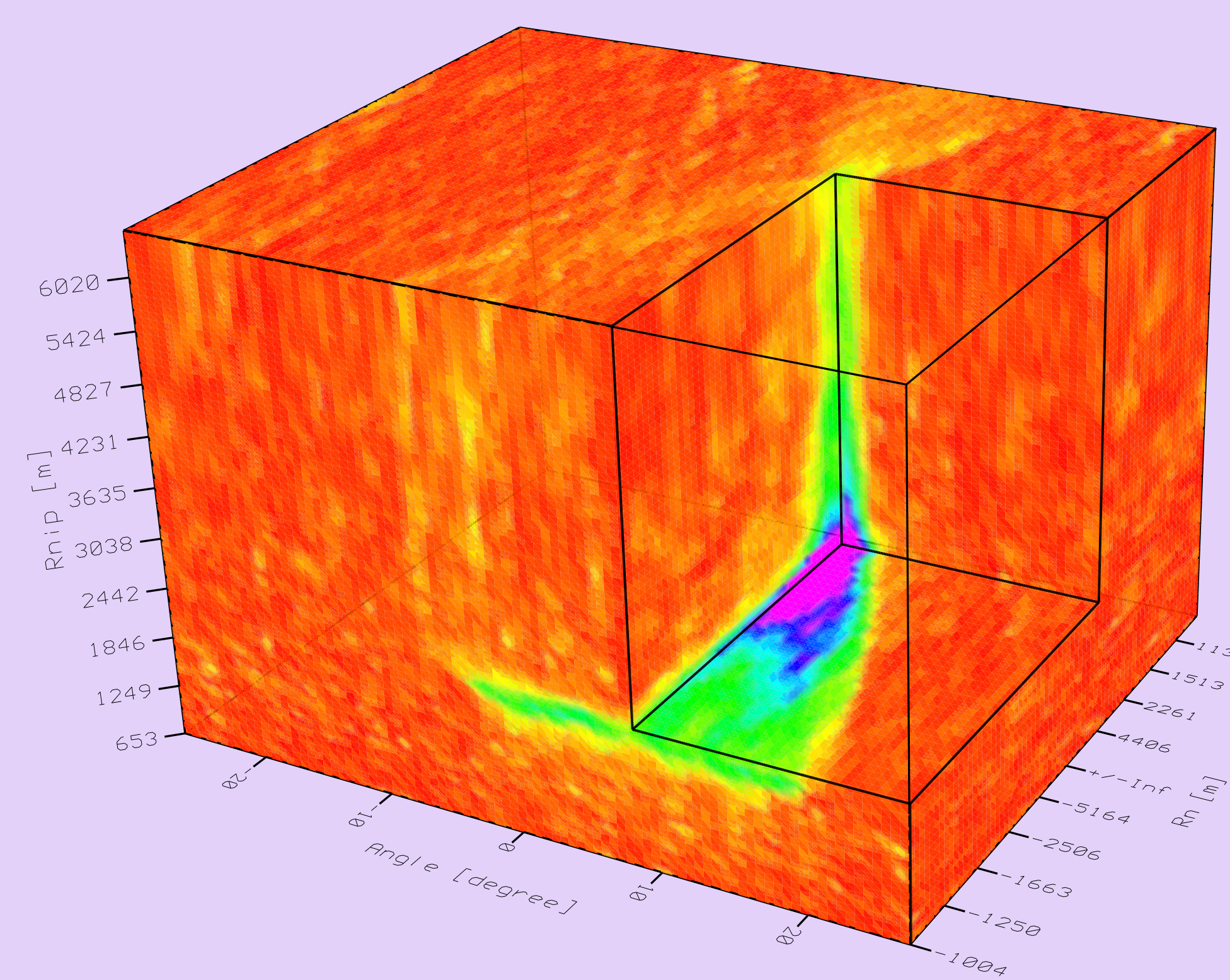


Figure 5: Coherency depending on the wavefront attributes for the point R depicted in Figure 3. The excavated block exposes the global maximum.

Another representation of the attribute domain is given with the cross sections in Figure 6. Due to the numerous local maxima it would be extremely time consuming to perform a three-parametric global optimization for each ZO sample to be simulated. For a more efficient determination of the wavefield attributes we split the procedure into separate steps.

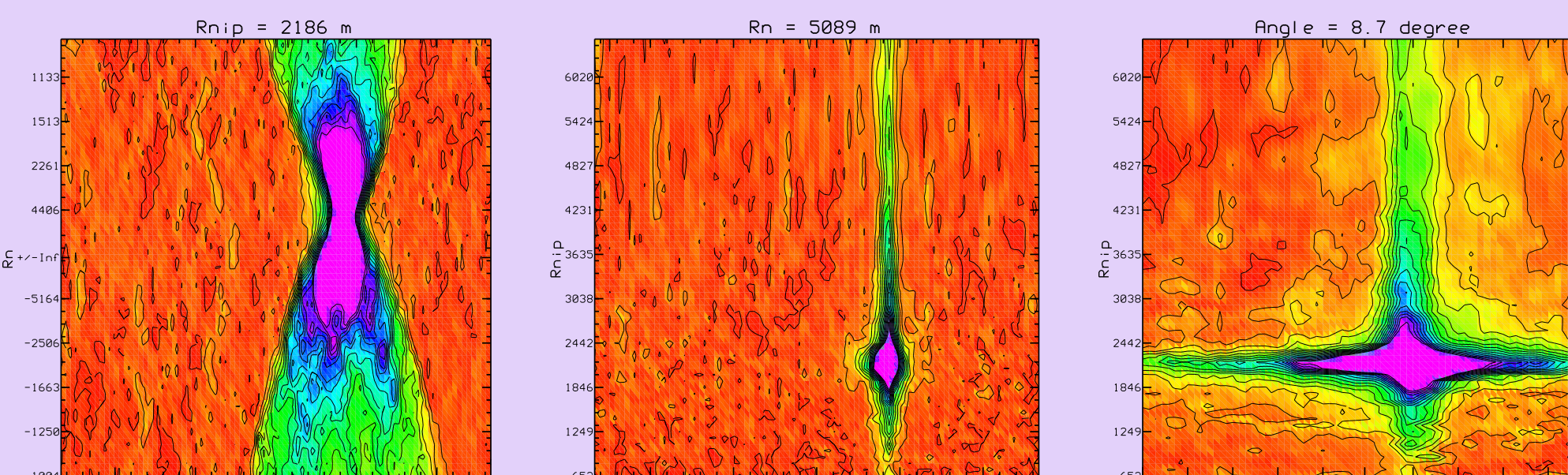


Figure 6: Cross sections through the maximum in the attribute domain shown in Figure 5.

Step I: automatic CMP stack

In the first step we search for the squared stacking velocity v_{NMO}^2 yielding the highest coherency in the CMP gathers. For this example we used the coherency criterion semblance. This one-parametric search can be easily performed on an appropriate grid, the resulting CMP stacked section is shown in Figure 7.

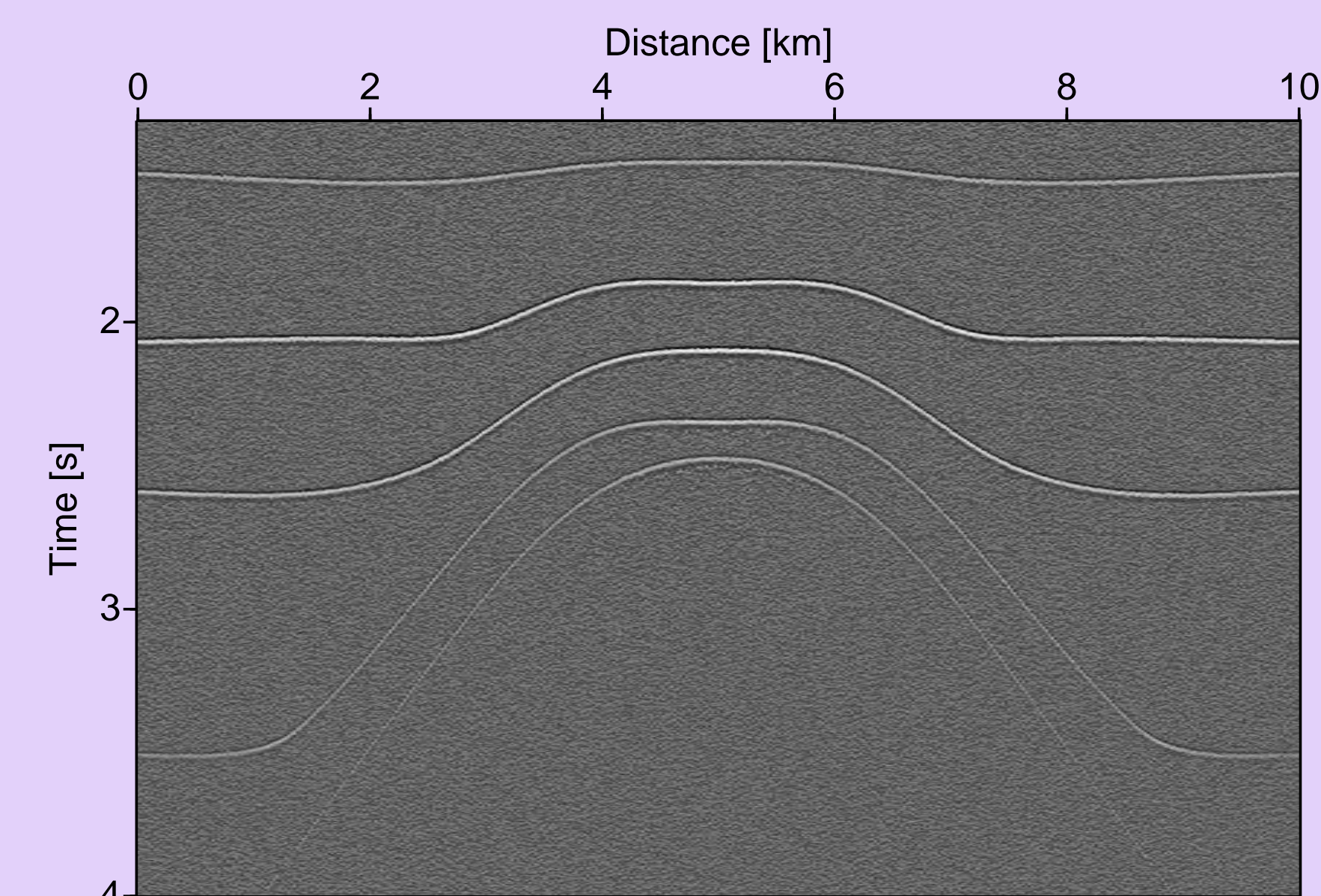


Figure 7: CMP stacked section automatically generated without velocity model. Only the near-surface velocity has to be provided.

In addition to the (intermediate) stack result we obtain the coherency section depicted in Figure 8. In this section all events can be clearly identified. In areas with low coherency values the multi-coverage data set contains no events with hyperbolic moveout.

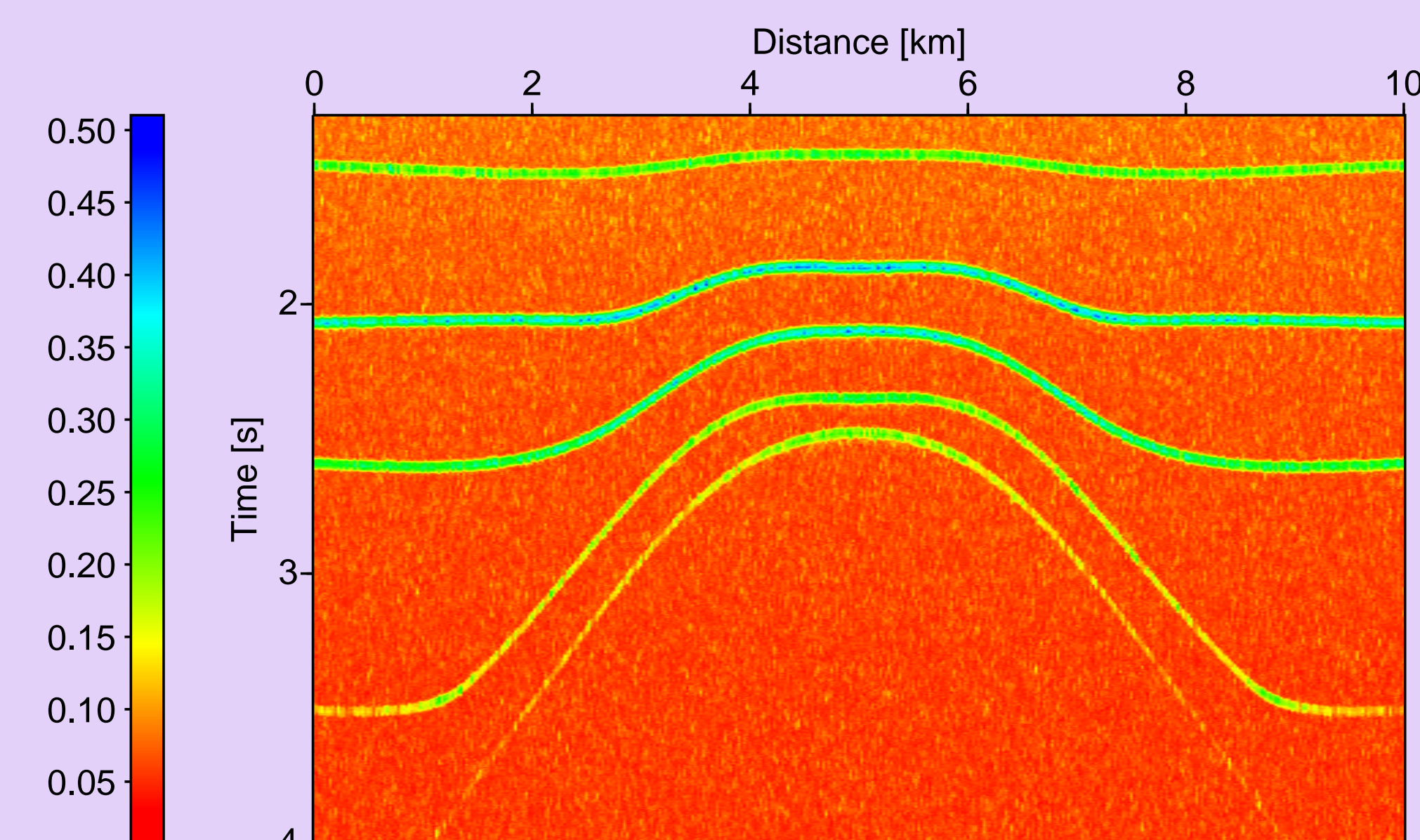


Figure 8: Coherency section associated with the CMP stacked section in Figure 7. All events have been detected.

The most exciting result of this processing step is the stacking velocity section displayed in Figure 9. Of course, the stacking velocity can only be successfully determined at the actual locations of the events, otherwise its value has no meaning.

Although no negative moveouts occur for the chosen model, the proposed method also accounts for imaginary stacking velocities corresponding to negative moveouts.

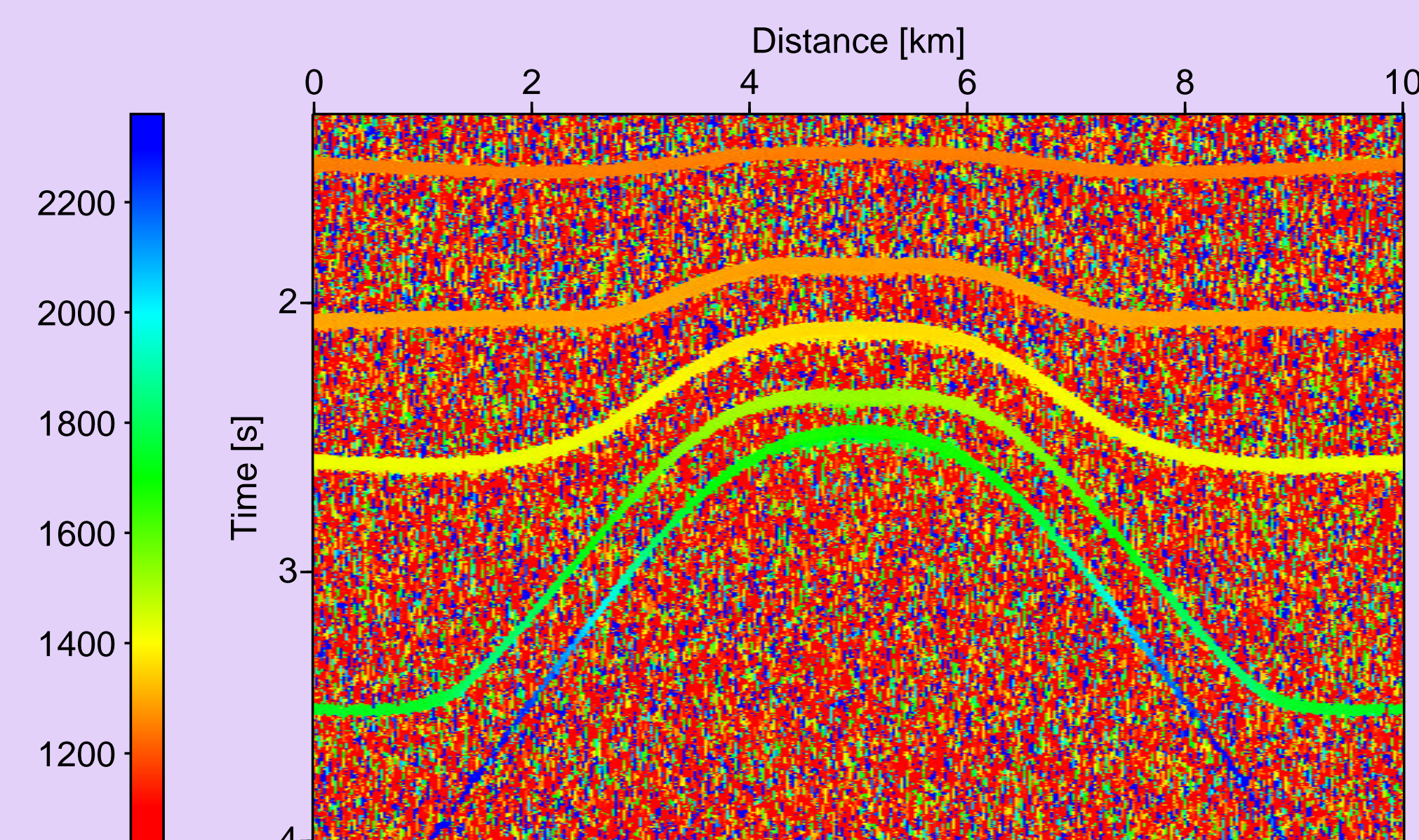


Figure 9: Stacking velocity v_{NMO} [m/s] determined during the automatic CMP stack.

The automatic CMP stack is an attractive and fast method to obtain a crude stacked section and a stacking velocity model. It does not require any macro velocity model but only the near-surface velocity.

If the data set contains strong multiples with hyperbolic moveouts (this was not simulated for this model), the search algorithm will possibly select multiple events for the stack. If these multiples can be identified in the stacking velocity section, the automatic CMP stack can be performed once again with appropriate constraints for the searched-for stacking velocities. In this way, primary events will be preferred.

As stated above for the CRS stacking operator, the squared stacking velocity v_{NMO}^2 only depends on the attributes α and R_{NIP} . With given stacking velocity, these attributes are no longer independent. Therefore, the following determination of the attributes reduces to a two-parametric search.

Step II: restricted CRS stack

With the stacking velocity determined in step I the number of independent attributes reduces to two. One possible way to continue is to apply the full CRS stacking operator with attributes restricted to the surface displayed in Figure 10. This surface is a subset of the attribute domain shown in Figure 5.

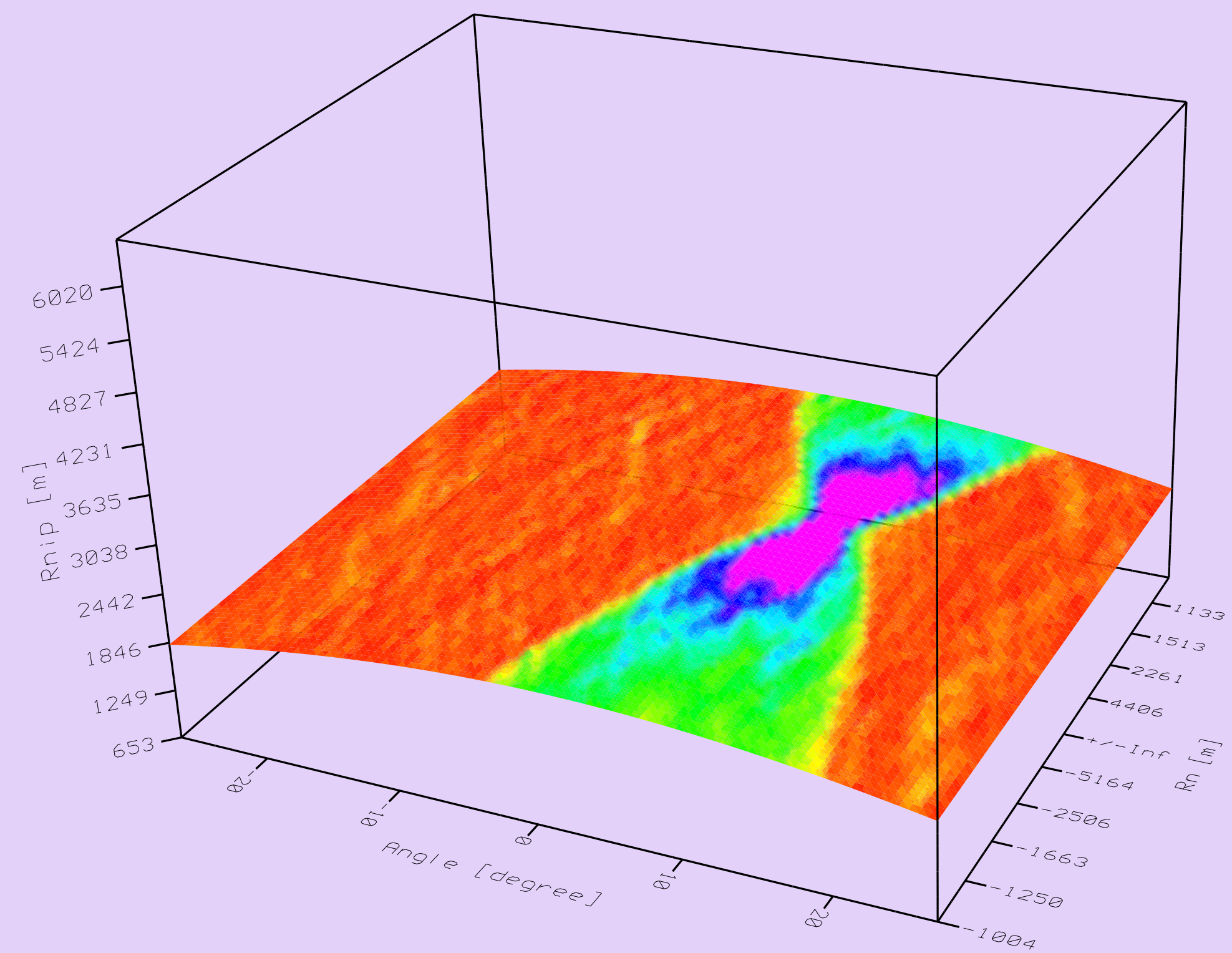


Figure 10: Coherency depending on the wavefront attributes for the point R depicted in Figure 3. The attribute domain is restricted according to the determined stacking velocity v_{NMO} .

Searching the maximum on a coarse grid on the surface in Figure 10, we obtain the stacked section shown in Figure 11, its associated coherency section (Figure 12), and intermediate sections of the attributes α , R_{NIP} , and R_N (not displayed).

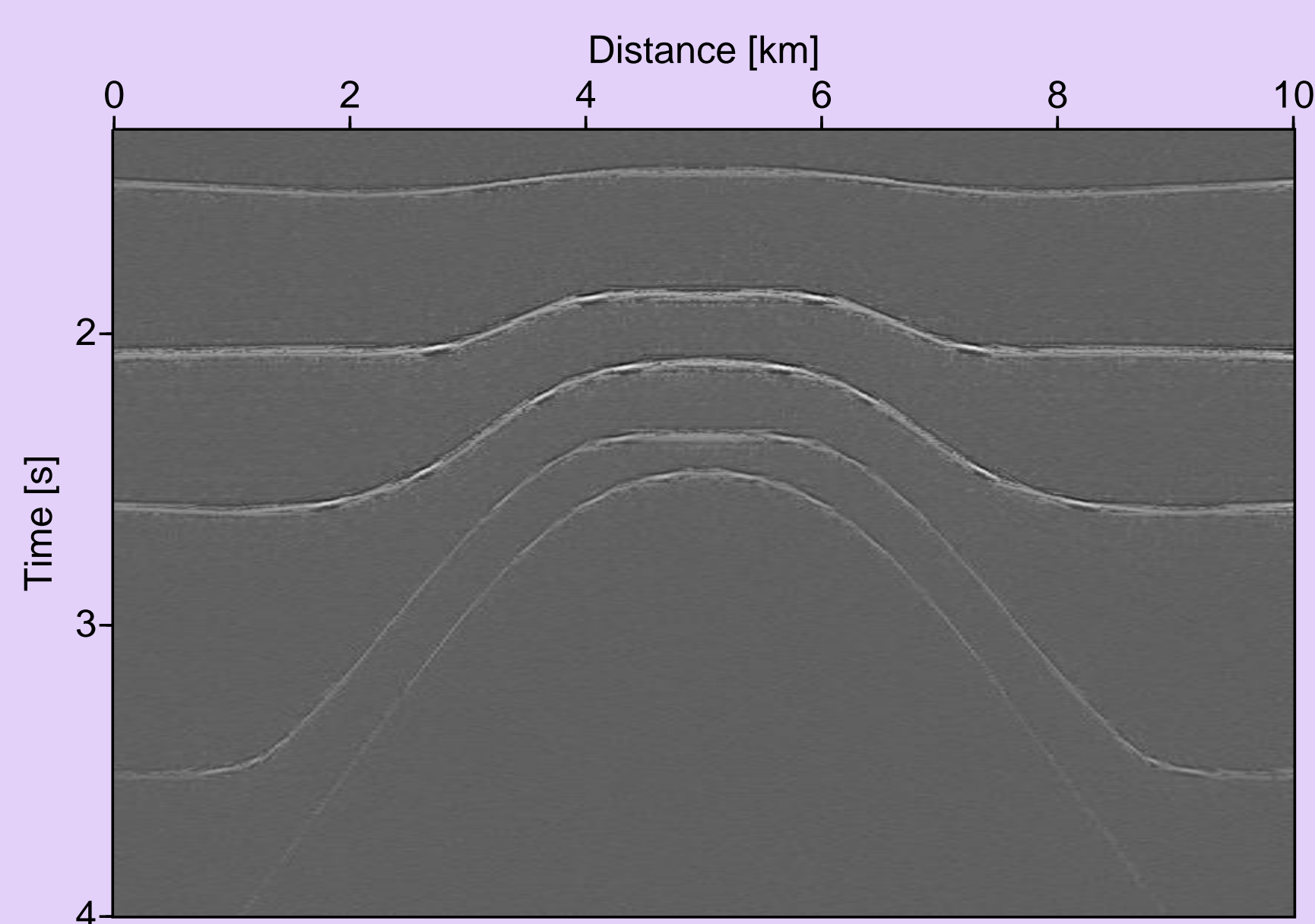


Figure 11: Stacked section generated by the restricted CRS stack.

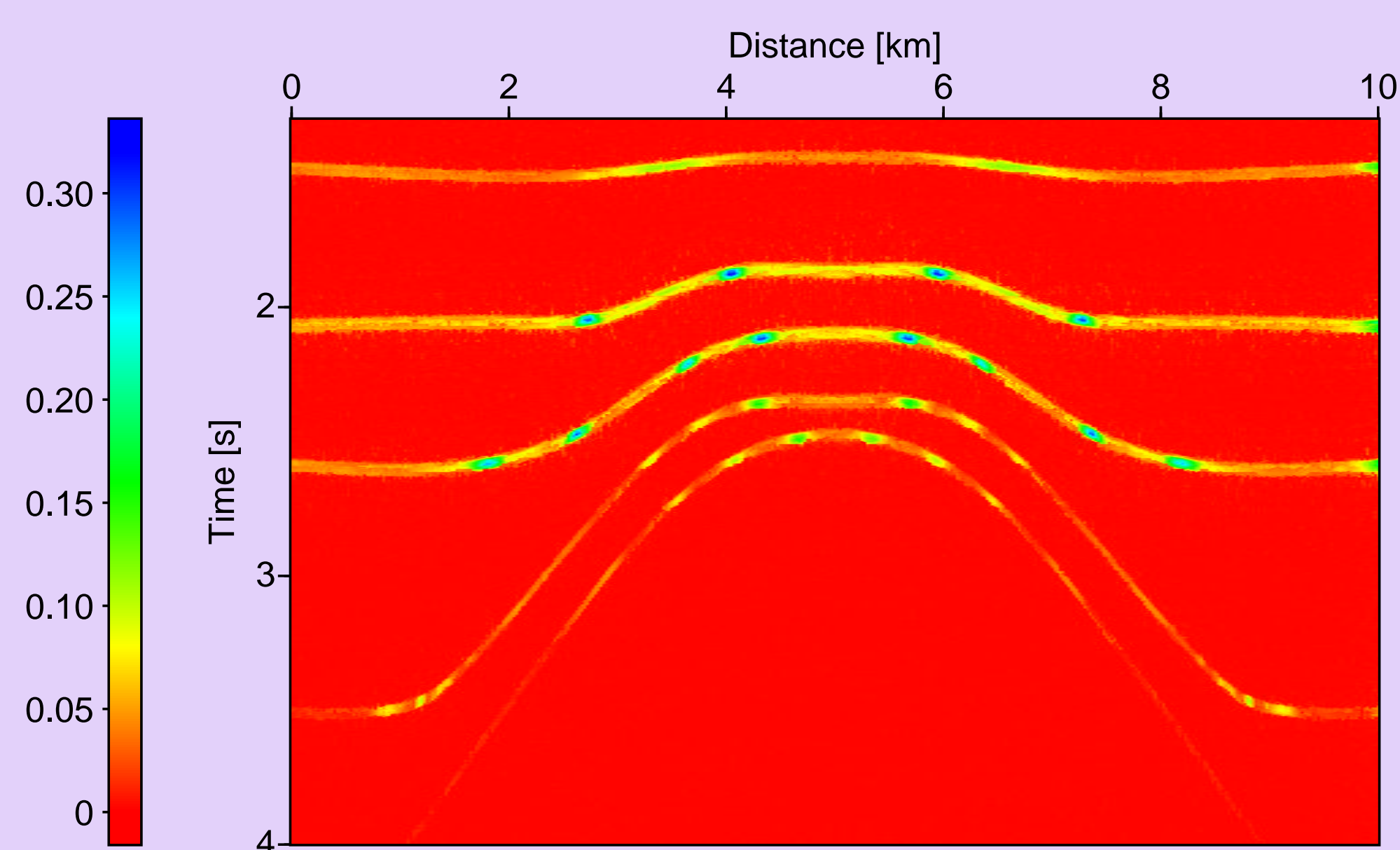


Figure 12: Coherency section associated with the stacked section shown in Figure 11.

Step III: Optimization

With the intermediate attributes obtained in step II we can expect to be already close to the global maximum in the respective attribute domain for each sample to be simulated. This enables us to perform a three-parametric local optimization algorithm, e.g. a flexible polyhedron search, to find the global maximum for each ZO sample: the results of step II are used as initial values. In this way, we obtain our final stack result: the optimized stacked section shown in Figure 13.

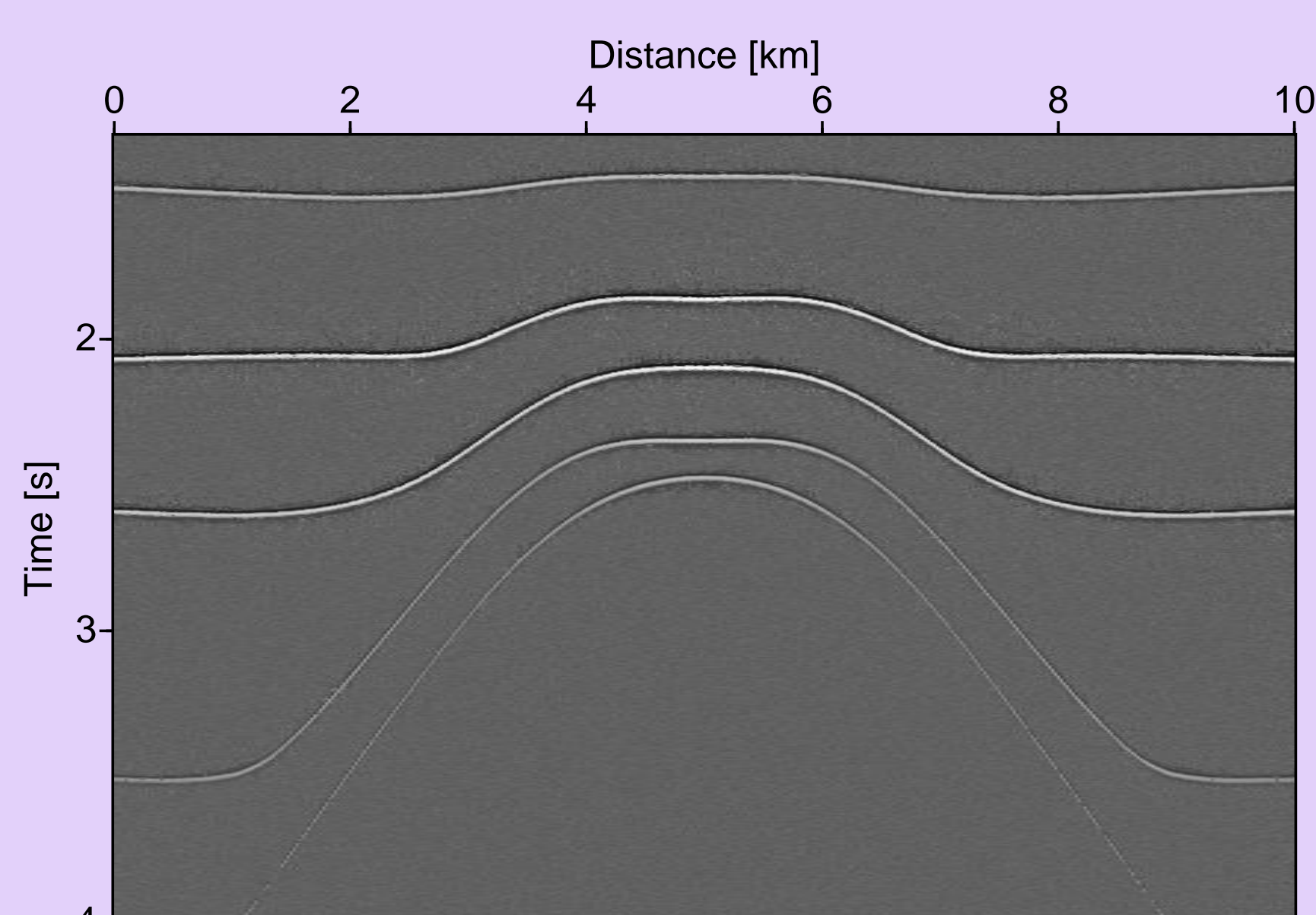


Figure 13: Stacked section as final result of the optimized CRS stack.

Wavefield attribute sections

In addition to the stacked section the CRS stack also yields the associated wavefield attributes sections for α (Figure 15), R_{NIP} (Figure 16), and R_N (Figure 17).

As stated for the stacking velocity section above, the attributes are only determined at the location of events which can easily be identified by means of the coherency section shown in Figure 14. Please notice the improvement of this coherency section compared to the coherency section of the restricted CRS stack in Figure 12.

According to Hubral and Krey (1980) the wavefield attributes can be used to derive an approximation of the 2-D macro velocity model. This would finally lead to an image in the depth domain.

For diffraction events (not included in this model) both radii of curvature coincide ($R_N = R_{NIP}$). This allows to separate reflection and diffraction events.

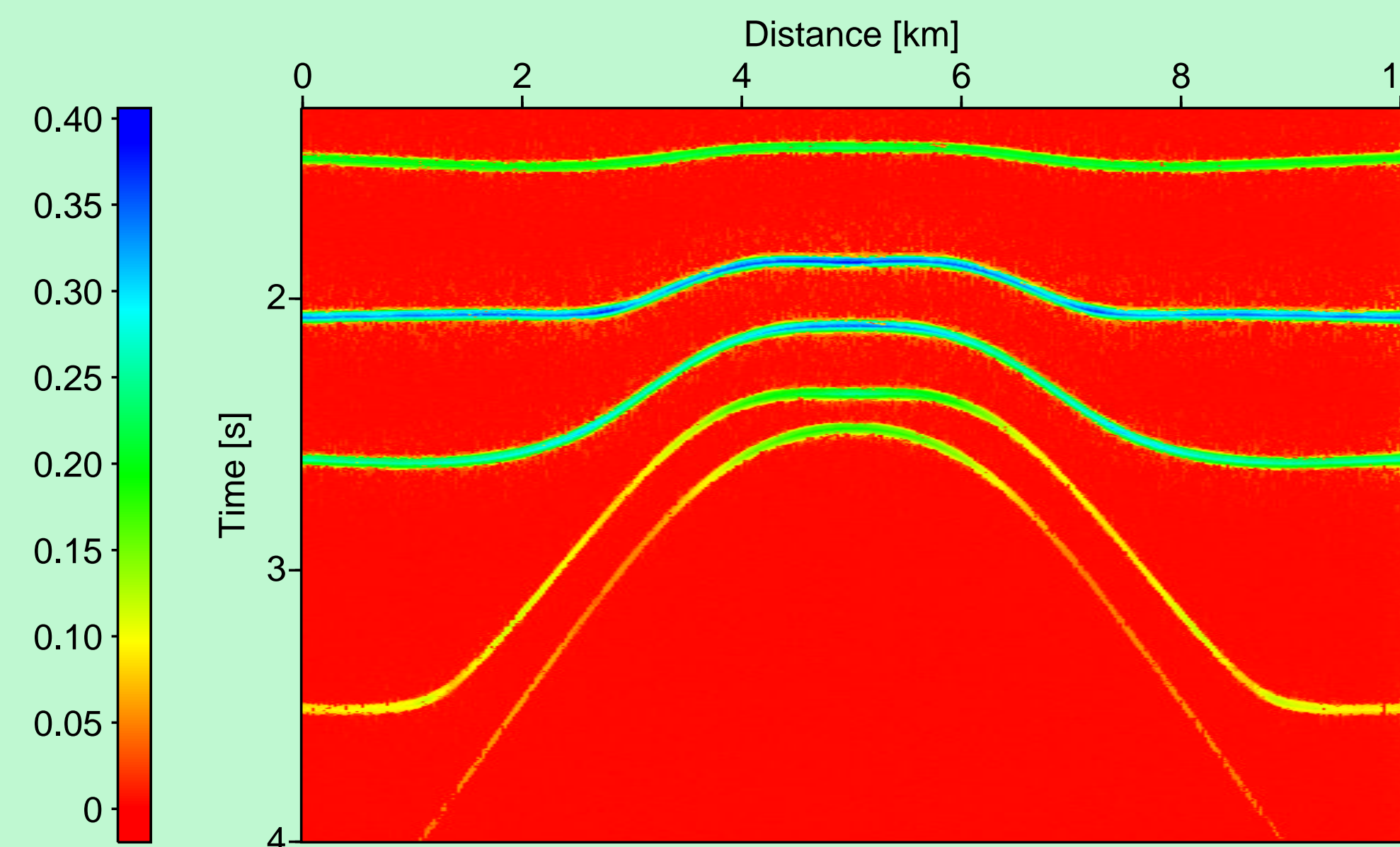


Figure 14: Coherency section associated with the optimized CRS stacked section in Figure 13. All events have been detected.

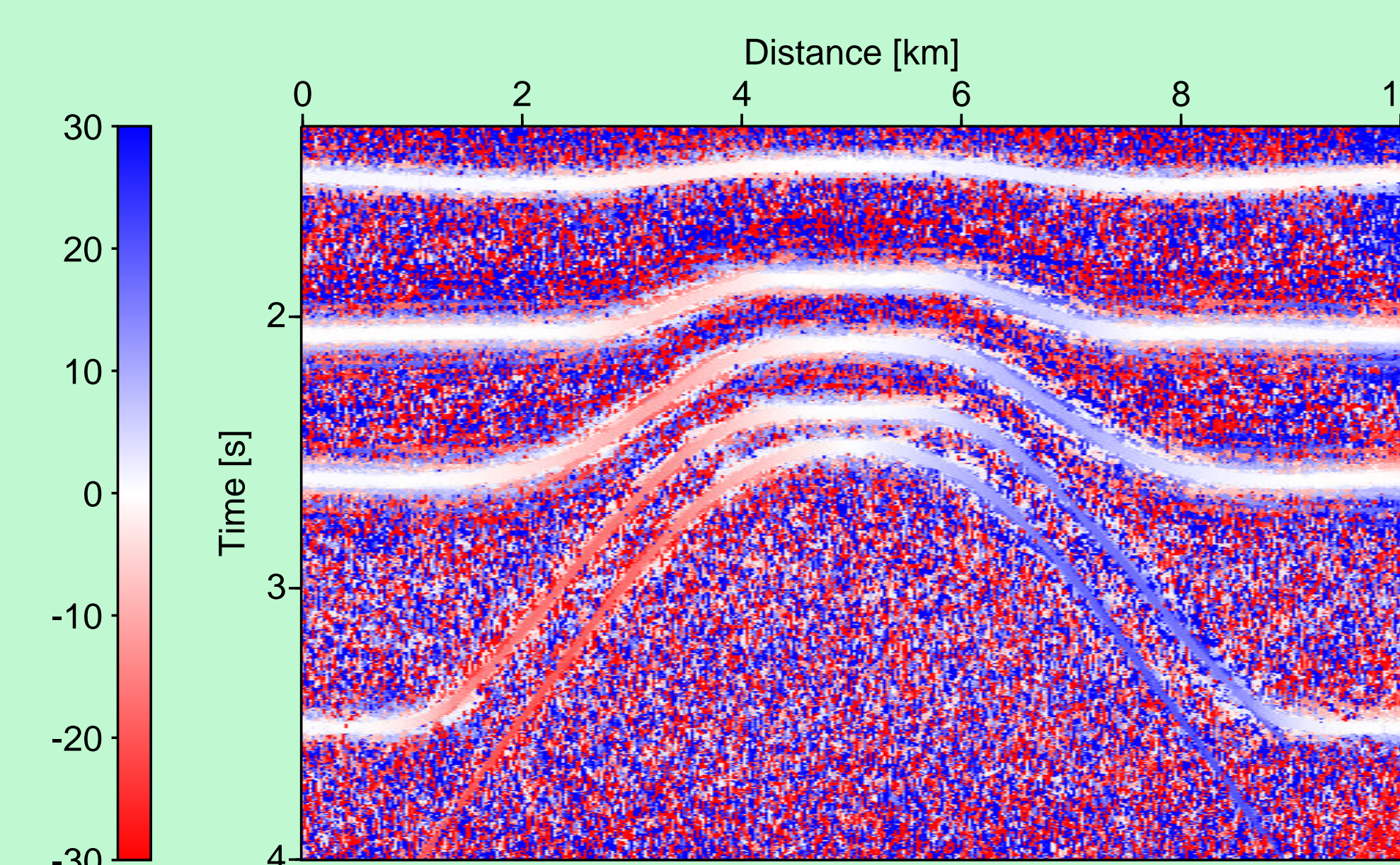


Figure 15: Emergence angle section [°] associated with the optimized CRS stacked section in Figure 13.

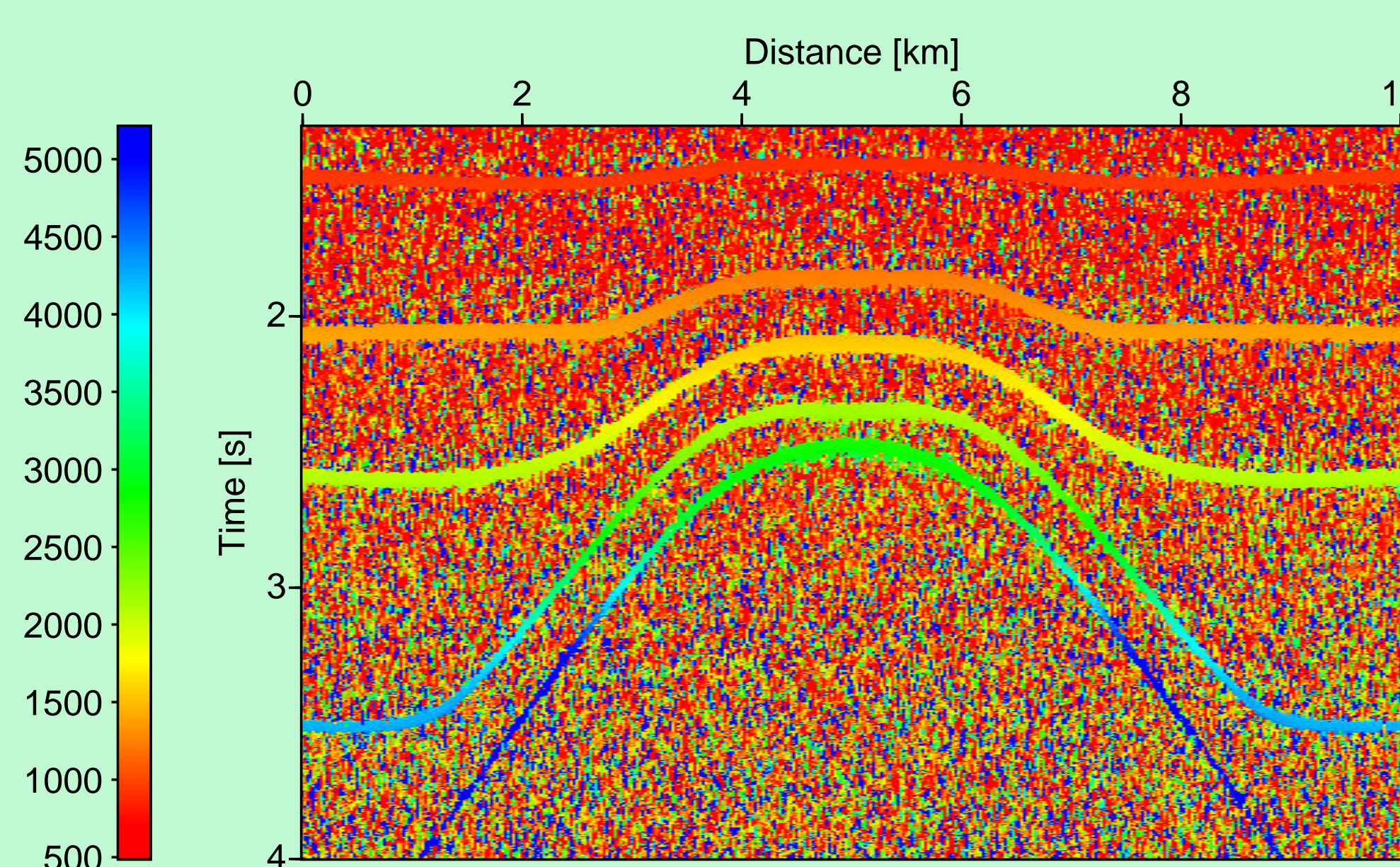


Figure 16: R_{NIP} section [m] associated with the optimized CRS stacked section in Figure 13.

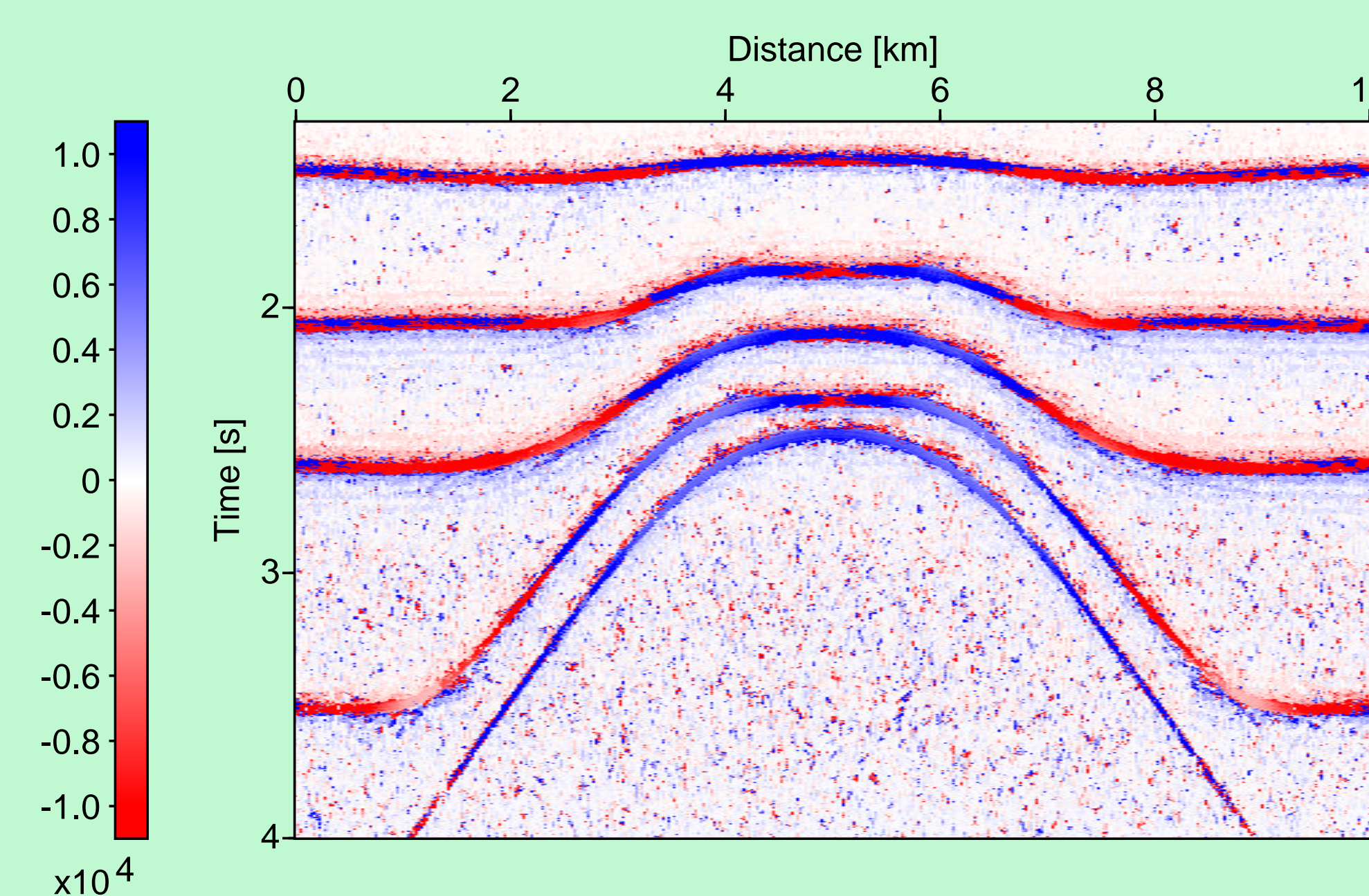


Figure 17: R_N section [m] associated with the optimized CRS stacked section in Figure 13.

Acknowledgements

This work was kindly supported by the *Wave Inversion Technology Consortium*, Karlsruhe, Germany and *Elf Exploration Production*, Pau, France.

Model-derived vs. data-derived attributes

In the figures below we compare the model-derived (forward calculated) wavefield attributes to the data-derived attributes. We observe a wide agreement, only for the deepest interface we obtained some drop-outs.

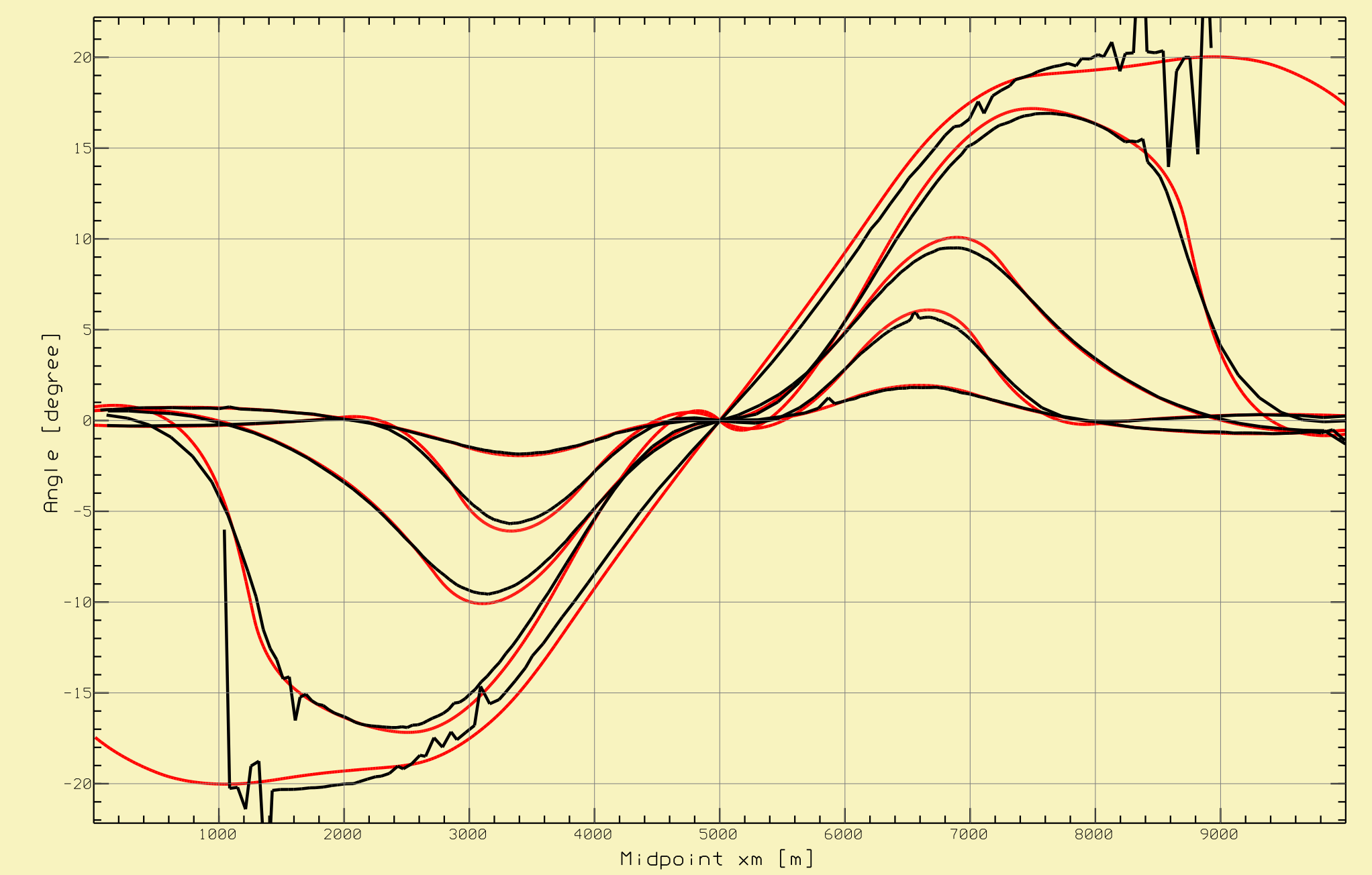


Figure 18: Model-derived (red) and data-derived (black) emergence angles for all layers.

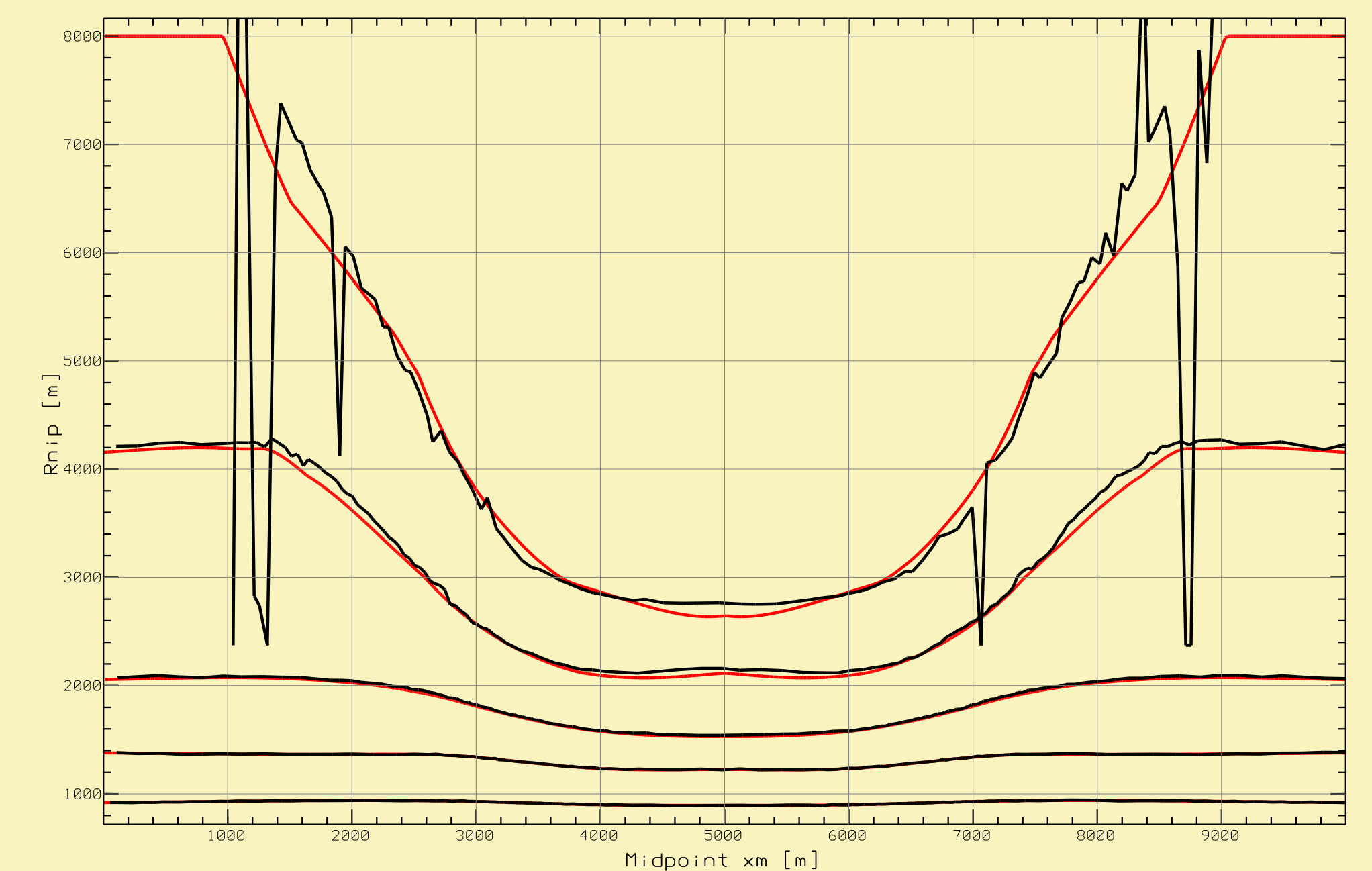


Figure 19: Model-derived (red) and data-derived (black) radii of curvature of the NIP waves for all layers.

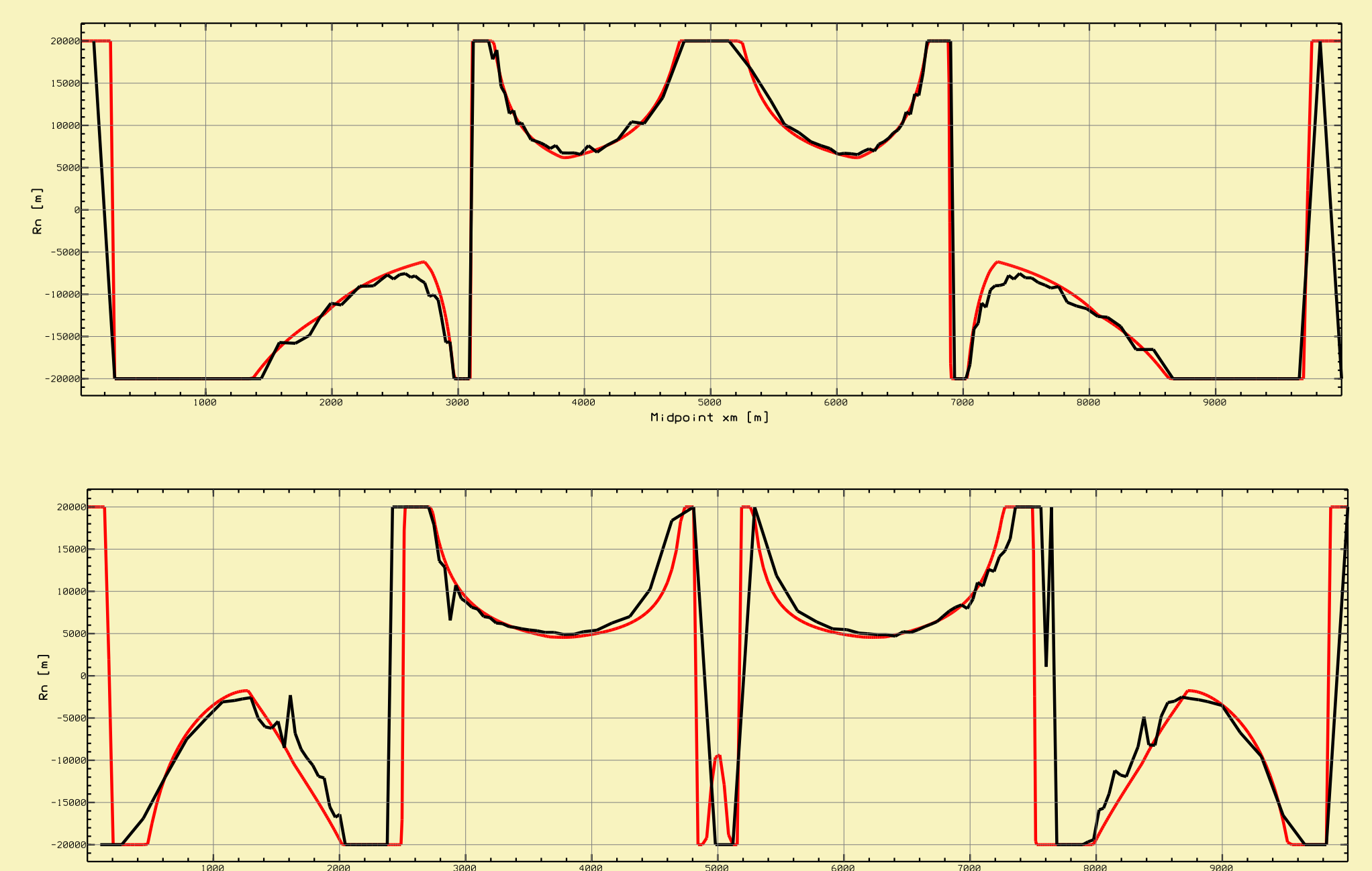


Figure 20: Model-derived (red) and data-derived (black) radii of curvature of the *normal* waves for the third and fourth layer.

Conclusions

The CRS stack is a model independent seismic imaging method and thereby can be performed without any ray tracing and macro velocity model estimation. Only the knowledge of the near surface velocity is required. As a result of a CRS stack one obtains in addition to each simulated ZO reflection time important wave-field attributes: the angle of emergence and the radii of curvature of the NIP and the *normal* wave.

The application to a synthetic dataset showed noteworthy results with respect to the stack section and the determined attributes. In view of the authors, the proposed strategies offer an exciting approach to improve the stack section and to allow for a subsequent inversion.

References

- Berkovitch, A., Gelchinsky, B., and Keydar, S., 1994, Basic formulae for multifocusing stack: 56th Mtg. Eur. Assoc. Expl. Geophys., Extended Abstracts, Session: P140.
- de Bazelaire, E., and Thore, P., 1987, Pattern recognition applied to time and velocity contours: 57th Annual Internat. Mtg., Soc. Expl. Geophys., Expanded Abstracts, Session: POS2.14.
- de Bazelaire, E., 1988, Normal moveout revisited – inhomogeneous media and curved interfaces: *Geophysics*, 53, no. 2, 143–157.
- Hubral, P., and Krey, T., 1980, Interval velocities from seismic reflection traveltimes measurements *: *Soc. Expl. Geophys.*
- Schleicher, J., Tygel, M., and Hubral, P., 1993, Parabolic and hyperbolic paraxial two-point traveltimes in 3D media: *Geophys. Prosp.*, 41, no. 4, 459–513.